A new numerical modeling for simulating the performance of a two-bed adsorption chiller based on adsorbent particle-level information

Mahmoud B. Elsheniti*, Mohamed A. Hassab, Abd-Elhamid Attia

Mechanical Engineering Department, Faculty of Engineering, Alexandria University, Alexandria, Egypt.

* **Corresponding author**

Abstract

A detailed 2-D axisymmetric transient model is developed to investigate the performance of a two-bed adsorption chiller utilizing silica gel/water pair. Transient distributed-parameter fully coupled model for a packed-bed adsorber is introduced employing the volume averaged Navier-Stokes equations. These equations are applied to describe the vapor flow in the adsorbent domain considering the inter-particle mass transfer, while the intra-particle mass transfer is modeled by the kinetic model and based on the confirmed isotherms data in literatures [1]. The condenser and evaporator are considered non-ideal and their energy balances and heat transfer equations are integrated with the beds' model through two time-dependent sub-models. The presented system of equations is numerically solved by using COMSOL Multiphysics software. For the given operating and physical parameters in this study, the simulations of the results showed that the chiller performance is considerably enhanced in case of the turbulent heat-transfer-fluid (HTF) flow compared to that in laminar HTF flow case. The average specific cooling capacity (SCC) and the coefficient of performance (COP) are examined with different cycle durations. As the turbulent HTF flow is considered, the maximum SCC is 282 W/kg$_{ads}$ at the shortest cycle times of 330 s and 440 s, while the COP is the smallest at those times (about 0.47), COP is increased with longer cycle durations to be about 0.61 at cycle time of 1140 s, while SCC is decreased to be 230 W/kg$_{ads}$. The heating energy during the pre-heating mode represents about 18 % of the total heat added that influenced by the sensible heat consumed in the beds.

***Keywords*:** adsorption chiller, packed-bed modeling, finned-tube adsorber and solar cooling.

1. Introduction

Man-made Global Warming has become an environmental priority around the world, and continuing using of conventional vapor-compression refrigeration systems aggravates this phenomenon through two ways: Firstly, direct emissions of fluorocarbon refrigerants which are classified as highly potent greenhouse gases with high Global Warm Potential (GWP). Secondly, indirect emissions of CO_2 emitted from power plants provide electricity to operate these conventional systems. Thermally-activated cooling technologies appear to be an alternative solution to the limited energy sources and ecological problems, where they can utilize directly thermal energies or recovery the waste heats as in combined cooling heating power (CCHP) systems, and use environmentally save refrigerants [2].

Nomenclature

COP	coefficient of performance
C_p	specific heat capacity (J/kg k)
d_p	adsorbent particle diameter (m)
D_s	surface diffusivity (m^2/s)
D_{so}	pre-exponent constant of surface diffusivity (m^2/s)
E_a	activation energy of surface diffusion (J/kg)
k	thermal conductivity (W/m K)
K	turbulent kinetic energy (J/kg)
$k_a s_p$	overall mass transfer coefficient (s^{-1})
K_o	pre-exponential constant in (Pa^{-1})
k_p	permeability (m^2)
LH	latent heat (J/kg)
M	mass (kg)
$\dot{m}$	mass flow rate (kg/s)
p	pressure (Pa)
Q	average heat rate (W)
Q_m	source term in mass balance equation (kg/m^3. s)
r	radial coordinate (m)
R	gas constant (J/kg K)
SCC	specific cooling capacity (W/kg_{ads})
T	temperature (^oC)
t	time (s)
t_1	dimensionless Tóth's constant
u	fluid velocity (m/s)
UA	heat transfer conductance (W/K)
w	specific adsorption (kg/kg_{ads})
w_{eq}	equilibrium adsorption uptake (kg/kg_{ads})
X_m	monolayer capacity (kg/kg_{ads})
z	axial coordinate (m)

Subscripts

ads	adsorbent
chw	chilled water
cond	condenser
cw	cooling water
e	equivalent
eva	evaporator
f	fluid
hw	heating water
i	inlet
l	liquid
m	metal
o	outlet
r	radial direction
rl	refrigerant liquid
rv	refrigerant vapor
s	solid adsorbent
v	vapor
z	axial direction

Greek symbols

ΔH_s	heat of adsorption (J/kg)
ε	effectiveness
ε_b	bed porosity
ε_T	total porosity
μ	viscosity ($N\ s/m^2$)
μ_T	turbulent viscosity($N\ s/m^2$)
ρ	density (kg/m^3)

Adsorption refrigeration systems, one of these heat-driven systems, have a distinct advantage in their ability to be driven by a relatively lower temperature heat sources as well as not involving any moving parts which means low maintenance and more durability. The researchers have been working on several investigations to make adsorption systems able to be applied effectively in many applications. These investigations include new and modified adsorbent-refrigerant working pairs, advanced cycle arrangements, and improvement the adsorbent-bed heat and mass transfer. As far as the coupling of the heat and mass transfer in the adsorbent bed were solved numerically, where the inter-particle and intra-particle mass transfer resistances were considered, the following papers were dealing with this context.

Sum el at. [3] indicated the importance of solving the mass transfer within the adsorbent, particularly, when the adsorber working under low pressures as in the case in which water and methanol are used as refrigerants, and thus using of uniform pressure model is erroneous in such cases. Chua el at. [4] confirmed the previous conclusion after comparing between a 'transient distributed-parameter model' which couples the heat and mass transfer in the adsorber and a 'lumped parameter model' was made by the same authors. They confirmed that the lumped-parameter model will under-predict the cooling capacity by 14%, when a cycle time of 850 s was taken as an example.

Sharafian el at. [5] studied experimentally the effects of fin spacing on the temperature distribution inside the adsorbent bed using two heat exchangers with fin spacing 9.5 mm and 6.35 mm. They observed that a greater reduction is existed in the temperature gradient inside the finned tube adsorbent-bed with smaller fin spacing.

Zhang and Wang [6] presented a numerical analysis of the performance of zeolite-water system driven by automobile waste heat. They concluded that parameters such as the fin numbers, the adsorbent thickness, and the heat transfer coefficients had a great impact on the system performance.

Leong and Liu [7] used the same pair and similar model approach in [6] without fins and found that performance can be strongly influenced by the adsorbent thickness and porosity of the adsorbent bed, while the variation of particle size has a minimal effect on the bed performance.

In more recent work introduced by Niazmand and Dabzadeh [8], the effects of bed configurations were examined. Results showed that fins in general reduce the COP of the system. However, for a given total cooling capacity, the bed size could be reduced dramatically with employing fins at the cost of slightly lower COP. As a connected work, Niazmand el at. [9] studied also the effects of using annular and square plate fins on others bed parameters.

Mehdi el at. [10] developed a three-dimensional non-equilibrium numerical model to investigate the performance of an adsorption chiller employed composite sorbent SWS-1L.While the evaporator and condenser were considered ideal in the last three papers, Liu and Leong [11] investigated by a transient two-dimensional model the effect of non-constant condenser pressure on the cycle duration and cycled adsorbate, which were increased compared with that in the ideal conditions.

Wang R. Z. et al. [12] examined two prototypes of adsorption systems. For the air conditioning prototype, the COP was ranged from 0.15 to 0.21 which was far lower than the theoretical estimated value of about 0.6. The authors explained the cause of the lower performance by a large heat capacity of the adsorber mass and the HTF.
Freni el at. [13] examined experimentally the utilization of novel composite water sorbent "silica modified by calcium nitrate" (SWS-8L) in a lab-scale adsorption chiller driven by low-temperature heat source. Experimental cooling COP was 0.18-0.31 at cycle time 10 min which was noticeably lower than estimated COP (0.51-0.71), the authors considered dynamic limitations of the adsorbent bed, parasitic losses, inert mass of the heat exchangers and vacuum chambers, etc. were the causes of the reduction in the actual COP. The two previous

experimental works give an example of the importance of theoretical studies that deal with the thermal mass of adsorber components before setting up prototypes.

It is noticed from the above reviewed papers that developing a more precise numerical model to be used in enhancing the performance of the adsorption refrigeration systems is strongly required. Essentially, such models can help in the best choice of the prototype configurations which minimize the time and cost of the experimental works. In this model, the dynamic thermal losses and other energy losses will be taken into consideration. Besides, simulating the time variations of the temperature, pressure, and equilibrium and instantaneous amount of adsorbate will help in clear understanding of the net effects of the variations in the design and operational parameters.

2. Description of The Adsorption System Model

This study is dedicated to simulate a conventional two-bed configuration adsorption cooling system. The system consists of two adsorbent-beds, a condenser, an evaporator and an expansion valve, in addition to the four connecting valves and connecting pipes. Each bed undergoes four modes of processes named as: pre-heating, heating (desorption), pre-cooling and cooling (adsorption) in repeated cycles, the flow diagram of the system is illustrated in Fig. 1 whereas desorption/adsorption mode is applied. The working principle of the basic cycle is discussed in details in reference [14]. In brief, while hot water is used to heating up Bed-A during the first two modes, cooling water is used to cooling down Bed-B. The hot water is switched to the Bed-B in the last two modes, as the Bed-A is subjected to cooling water. The four valves are completely closed during the two switching pre-heating and pre-cooling modes. Circulating the cooling water and chilled water in the condenser and evaporator respectively are supposed to be continuous during the whole cycle.

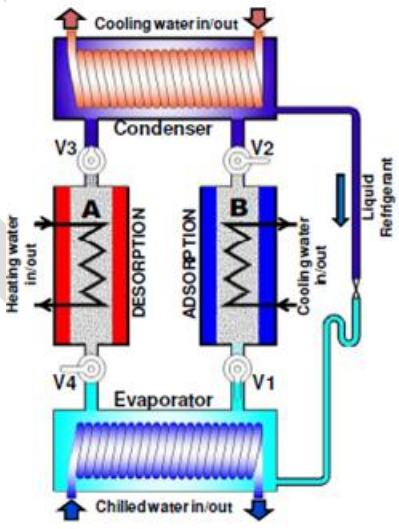

Fig. 1. Schematic diagram for a conventional two-bed adsorption chiller, as Bed-A in desorption mode, Bed-B in adsorption mode [15].

3. Mathematical model

Each one of the modeled adsorber is packed with 10 kg of adsorbent; therefore about 95 tubes (modules) are used to match the physical parameters of the simulated model given in Table 1. To avoid the complexity in solving the 3-D transient model for one module shown in Fig. 2(a), a 2-D axisymmetric transient model is introduced in this study based on the symmetry property of the cylindrical geometry in the tangential direction as shown in Fig. 2(b). The inlet and outlet openings are considered on whole side area to match the symmetry of the complete shape, so that the opening of each adsorber that is given in the 2-D axisymmetric model will be considered inlet or outlet depending on the mode of operation.

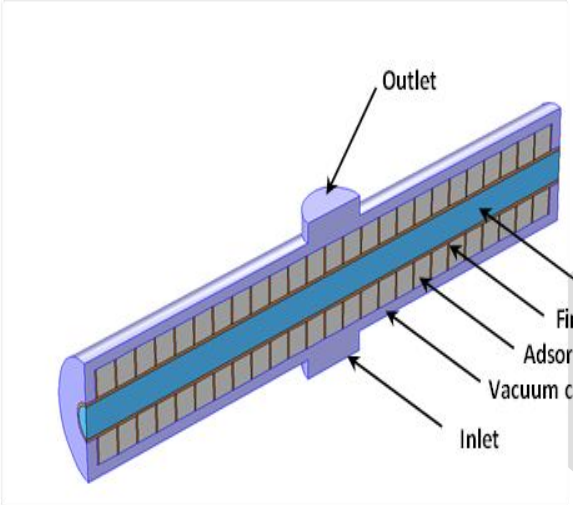

Fig. 2(a). Physical configurations of the main domains for the adsorbers' module.

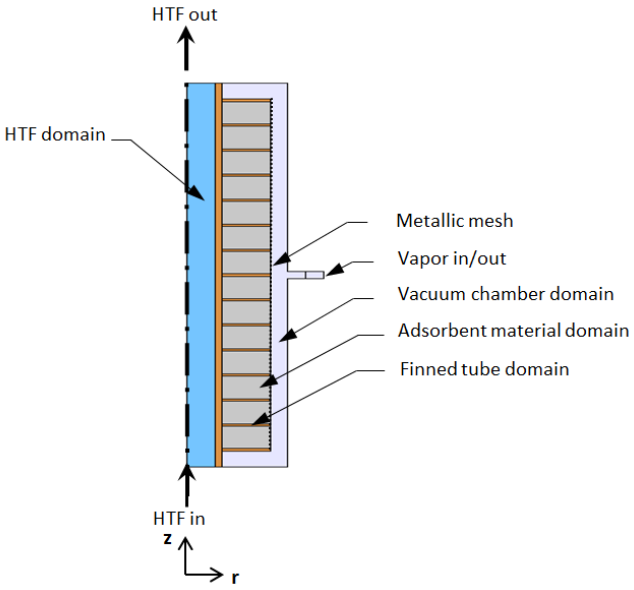

Fig. 2(b). The 2-D axisymmetric control volumes considered in the study and their corresponding four domains for one module.

3.1 Assumptions

The continuum equations governing the main four domains of the adsorber are adjusted in COMSOL Multiphysics while the following assumptions are accounted:

1. The three phases of the adsorbent domain are in a local thermal equilibrium.
2. The volume occupied by the adsorbate phase is neglected.
3. Vapor phase behaves as an ideal gas.
4. Specific heat of the adsorbate is considered to be of liquid phase.
5. Adsorbent domain is considered as a continuous media and hence conduction heat transfer in the porous media can be characterized by an equivalent thermal conductivity.
6. Adsorbent particles have identical properties and are uniformly distributed in the bed, i.e. the porous media is homogeneous and isotropic.

7. Viscous dissipation, radiative effects and the work done by pressure changes are negligible.
8. Heat of adsorption is considered constant throughout the adsorbent domain.

3.2 Governing equations

HTF domain equations

The conservation of energy equation for the HTF can be given as follows:

$$\rho_f C_{pf} \frac{\partial \mathrm{T}_f}{\partial t} + \rho_f C_{pf} u_{f,z} \frac{\partial \mathrm{T}_f}{\partial z} + \rho_f C_{pf} u_{f,r} \frac{\partial \mathrm{T}_f}{\partial r} = \frac{\partial}{\partial z}\left(k_f \frac{\partial \mathrm{T}_f}{\partial z}\right) + \frac{1}{r}\frac{\partial}{\partial r}\left(r\, k_f \frac{\partial \mathrm{T}_f}{\partial r}\right) \quad (1)$$

The conservation of mass for the HTF can be described as follows:

$$\rho_f \nabla . u_f = 0 \quad (2)$$

According to the given data of the flow inside the HTT, in case of laminar flow, The Navier-Stokes equations for incompressible flow are given as:

$$\rho_f \frac{\partial u_f}{\partial t} + \rho_f (u_f . \nabla) u_f = -\nabla p \boldsymbol{I} + \nabla . \left[\mu \left(\nabla u_f + \left(\nabla u_f\right)^T\right)\right] \quad (3)$$

However, In case of turbulent flow, the RANS equations take the following form:

$$\rho_f \frac{\partial u_f}{\partial t} + \rho_f u_f . \nabla\left(u_f\right) = -\nabla p \boldsymbol{I} + \nabla . \left[(\mu + \mu_T)\left(\nabla u_f + \left(\nabla u_f\right)^T\right) - \frac{2}{3}\rho_f \boldsymbol{\kappa} \boldsymbol{I}\right] \quad (4)$$

$$\rho_f \nabla . u_f = 0$$

The $\boldsymbol{\kappa} - \varepsilon$ turbulence model is used to calculate the turbulent viscosity (μ_T) and the turbulent kinetic energy ($\boldsymbol{\kappa}$), while the model is modified by the wall functions to increase the accuracy of the model nearer to a solid wall.

HTT and fins domains equations

The energy is transferred through the heat transfer tube (HTT) by only the conduction heat transfer; then the conservation of energy for the metal tube is given by:

$$\rho_m C_{pm} \frac{\partial T_m}{\partial t} = \frac{\partial}{\partial z}\left(k_m \frac{\partial T_m}{\partial z}\right) + \frac{1}{r}\frac{\partial}{\partial r}\left(r\, k_m \frac{\partial T_m}{\partial r}\right) \quad (5)$$

Energy balance equation of the fins will take the same form of the equation (5), while they are made of aluminum to minimize the thermal capacitance of the adsorber.

Adsorbent material domain equations

The conservation of refrigerant mass in the adsorbent domain can be described as follows [16]:

$$\varepsilon_T \frac{\partial \rho_v}{\partial t} + \frac{1}{r}\frac{\partial (r\rho_v u_r)}{\partial r} + \frac{\partial (\rho_v u_z)}{\partial z} + (1-\varepsilon_T)\,\rho_s \frac{\partial w}{\partial t} = 0 \tag{6}$$

The momentum equations for the vapor flow in adsorbent domain can be expressed as:

$$\frac{\rho_v}{\varepsilon_T}\left[\frac{\partial u}{\partial t} + \frac{1}{\varepsilon_T} u.\nabla(u)\right] = \nabla\left[-pI + \frac{\mu}{\varepsilon_T}(\nabla u + (\nabla u)^T) - \frac{2}{3}\frac{\mu}{\varepsilon_T}(\nabla . u)I\right] - \left[\frac{\mu}{k_p} + \frac{Q_m}{\varepsilon_T^2}\right]u \tag{7}$$

The permeability k_p can be obtained from the semi-empirical Blake–Kozeny equation as:

$$k_p = \frac{d_p^2 \varepsilon_b^3}{150(1-\varepsilon_b)^2} \tag{8}$$

The energy balance for the adsorbent domain can be given by employing the volume averaging technique as:

$$\left[\left((1-\varepsilon_T)\,\rho_s C_{ps} + \varepsilon_t \rho_v C_{pv} + (1-\varepsilon_T)\,\rho_s w\, C_{pa}\right)\frac{\partial T_s}{\partial t}\right] + \frac{1}{r}\frac{\partial (r\rho_v C_{pv} u_r T_s)}{\partial r} + \frac{\partial (\rho_v C_{pv} u_z T_s)}{\partial z} = \frac{1}{r}\frac{\partial}{\partial r}\left(r\, k_e \frac{\partial T_s}{\partial r}\right) + \frac{\partial}{\partial z}\left(k_e \frac{\partial T_s}{\partial z}\right) + (1-\varepsilon_T)\,\rho_s \Delta H_s \frac{\partial w}{\partial t} \tag{9}$$

The pressure distribution takes place inside the adsorbent bed for the vapor flow through the change in the vapor density. The working pair examined in the present study is silica gel-water pair which is operated under vacuum conditions. Water vapor behaves as an ideal gas in low pressure conditions and its density can be calculated by ideal gas relation:

$$P = \rho_v R_v T_s \tag{10}$$

Vacuum chamber domain equations

Mass balance equation

$$\frac{\partial \rho_v}{\partial t} + \nabla(\rho_v u) = 0 \tag{11}$$

Momentum balance equations

$$\rho_v \frac{\partial u}{\partial t} + \rho_v u.\nabla(u) = -\nabla p I + \nabla.\left[\mu(\nabla u + (\nabla u)^T) - \frac{2}{3}\mu(\nabla . u)I\right] \tag{12}$$

Energy balance equation

$$\frac{\partial (\rho_v C_{pv} T_v)}{\partial t} + \nabla\left(\rho_v C_{pv} u\, T_v\right) - \nabla(k_v \nabla T_v) = 0 \tag{13}$$

Evaporator model equations

The energy balance and heat transfer equations of the evaporator can be written in the form of equations (14) and (15), respectively as: [17].

$$\left[M_{eva,rl}\, C_{p,eva,rl} + M_{eva,met}\, C_{p,eva,met}\right]\frac{dT_{eva}}{dt} = \dot{m}_{chw}\, C_{p,chw}\, \varepsilon_{eva}\left(T_{chw,i} - T_{eva}\right) - (1 - \alpha)\, \dot{m}_{v,eva}\, N_{tube,adsorber}\, \left[LH_{eva} - C_{p,rl}(T_{cond} - T_{eva})\right] \quad (14)$$

$$\varepsilon_{eva} = 1 - exp\left(\frac{-UA_{eva}}{\dot{m}_{chw}c_{chw}}\right) \quad (15)$$

Condenser model equations

Incorporating the overall energy balance with heat transfer equation for the condenser can be given, in a similar manner to that of evaporator, by the following equations [17]:

$$\left[M_{cond,rl}\, C_{p,cond,rl} + M_{cond,met}\, C_{p,cond,met}\right]\frac{dT_{cond}}{dt} = -\dot{m}_{cw}\, C_{p,cw}\, \varepsilon_{cond}\left(T_{cond} - T_{cw,i}\right) + (1 - \beta)\, \dot{m}_{v,cond}\, N_{tube,adsorber}\, \left[LH_{cond} + C_{p,rv}\left(T_{vap,out} - T_{cond}\right)\right] \quad (16)$$

$$\varepsilon_{cond} = 1 - exp\left(\frac{-UA_{cond}}{\dot{m}_{cw}C_{p,cw}}\right) \quad (17)$$

Adsorption equilibrium and kinetics model

X. Wang et al [1] investigated experimentally the using of Tóth's equation in predicting the equilibrium data of type 'RD' silica gel uptake characteristics. They found a very good agreement with the experimental and manufacturer's data by adjusting the equation parameters. The form of Tóth's equation was given as:

$$w_{eq} = \frac{K_o\, .exp[\Delta H_s/(R.T)].p}{[1 + \{K_o/X_m\, .exp[\Delta H_s/(R.T)].p\}^{t_1}]^{1/t_1}} \quad (18)$$

The adsorption/desorption rate $(\frac{dw}{dt})$ is defined by the classical linear driving force (LDF) model which was established by Sakoda and Suzuki [18] for the silica gel–water combination as:

$$\frac{dw}{dt} = K_s a_p (w_{eq} - w) \quad (19)$$

Where $K_s a_p$ is the overall mass transfer coefficient for the adsorption/desorption process within the particle (intra-particle mass transfer), and it is expressed by the following empirical equation [19]:

$$K_s a_p = \frac{F_o D_s}{Rp^2} \quad (20)$$

The adsorption rate is controlled by surface diffusion inside gel particle, and the equivalent surface diffusivity in the adsorbent particles D_s can be expressed by Arrhenius equation as a function of the temperature as follows:

$$D_s = D_{s0} exp\left(-\frac{E_a}{RT}\right) \quad (21)$$

Performance indicators

The results for the refrigerator cooling and heating capacities given next by equations (21) and (22) respectively; are used to evaluate this adsorption system performance defined by SCC and COP, written as:

$$Q_{eva} = \frac{1}{t_{cycle}} \int_0^{t_{cycle}} \dot{m}_{chw}\, c_{chw} \left(T_{chw,i} - T_{chw,o}\right)\, dt \quad (21)$$

$$Q_{heat} = \frac{1}{t_{cycle}} \int_0^{t_{cycle}} \dot{m}_{hw}\, c_{hw} \left(T_{hw,i} - T_{hw,o}\right)\, dt \quad (22)$$

$$SCC = \frac{Q_{eva}}{M_s} \quad (23)$$

$$COP = \frac{Q_{evap}}{Q_{heat}} \quad (24)$$

4. Numerical method and validation

The equations described in the last section are numerically solved by utilizing COMSOL Multiphysics software package which is based on the finite element technique. The model equations are adapted to COMSOL using six different Physics: The Heat Transfer Physics that couples the transport of heat throughout all the adsorbers domains; the Free and Porous Media Flow Physics for modeling mass and momentum balances in adsorbent and vacuum chamber domains; the Convection-Diffusion Equation for LDF model; the two Ordinary Differential Equations for condenser and evaporator model which are applied at the boundaries of each

adsorber (vapor openings); and the Turbulent Flow (k-ε) Physics for HTF flow in case of turbulent flow.

Table 1. Values of parameters employed in simulating the adsorption model.

Parameter	Symbol	value	Reference
Adsorbent bed reactor Adsorbent material Fuji Davison RD Silica gel			
Adsorbent mass	M_{sg}	10 kg per adsorber	
Average particle diameter	R_p	1.7×10^{-4} m	[20]
Skeleton density	ρ_s	2027 kg/m^3	[4]
Specific heat of adsorbent	C_{ps}	924 J/kg K	[4]
thermal conductivity of silica gel	k_s	0.198 W/m K	
Heat of adsorption	ΔH_s	$2.695 * 10^6$ J/kg	[4]
Bed porosity	ε_b	0.3955	
Total porosity	ε_T	0.65466	
Heat transfer tube HTT Bare copper tube			
HTT material density	ρ_m	8930 kg/m^3	
HTT material specific heat	C_{pm}	386 J/kg K	
Adsorber tube length	L	400 mm	
Inner radius of HTT	R_{ti}	3.15 mm	
Outer radius of HTT	R_{to}	3.96 mm	
Number of HTT	N_{tube}	95 per adsorber	
Fins Annular aluminum fins			
Fins material density	ρ_{fin}	2700 kg/m^3	
Fins material thermal conductivity	k_{fin}	160 W/m K	
Fins material specific heat	C_{pfin}	900 J/kg K	
Fins height	H_f	8 mm	
Fins spacing	L_s	3.8 mm	
Fin thickness	δ	0.2 mm	
Number of fins	N_{fin}	100	
Vacuum chamber space	L_{ch}	2 mm	
Vapor in/out opening length	L_{op}	8 mm	

The mesh types used in the model geometry have been set up by Physics-Controlled Mesh with finer element size option in COMSOL. The total number of elements was 332970 with an average element quality 0.8. This option takes into account the types of equation solved in each domain and the boundary conditions to improve the solution where variables may have large gradients.

The model has been validated with the experimental data published in reference [20] for HTF outlet temperatures of type RD silica gel and water based chiller. Fig. 3 compares the temperature histories for HTF at the outlet of the adsorber, of our presented model, with the experimental data of one adsorber established by the authors of reference [80] considering the same available values for the system configurations and operating conditions. It is obvious that the simulation results of the developed model in this study exhibit good agreement with the experimental data.

5. Results and discussions

Fig. 3. Comparison between the time variation of HTF outlet temperature for Bed-A in the present study with its corresponding experimental temperature in reference [20].

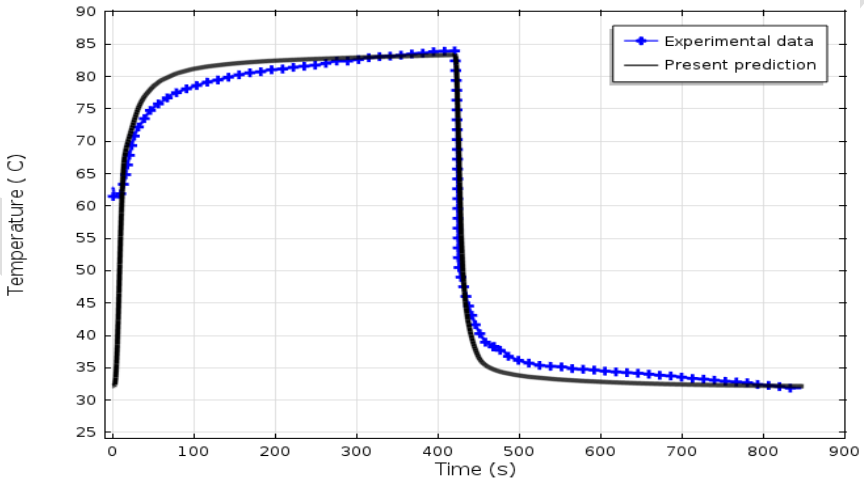

Fig. 3. Comparison between the time variation of HTF outlet temperature for Bed-A in the present study with its corresponding experimental temperature in reference [20].

It is known that an ARS performance is considerably influenced by the cycle time, while the best cycle time for given configurations and operating conditions may be not the same. Therefore, the effect of the cycle time on the performance of the given model is studied and illustrated in Fig. 4 by considering the two cases of the HTF: laminar flow and turbulent flow. Fig. 4 shows the variations of the average chiller specific cooling capacity SCC and COP after reaching the steady state of the cycle with different cycle durations, as the velocities of HTF were taken as in Table 2.

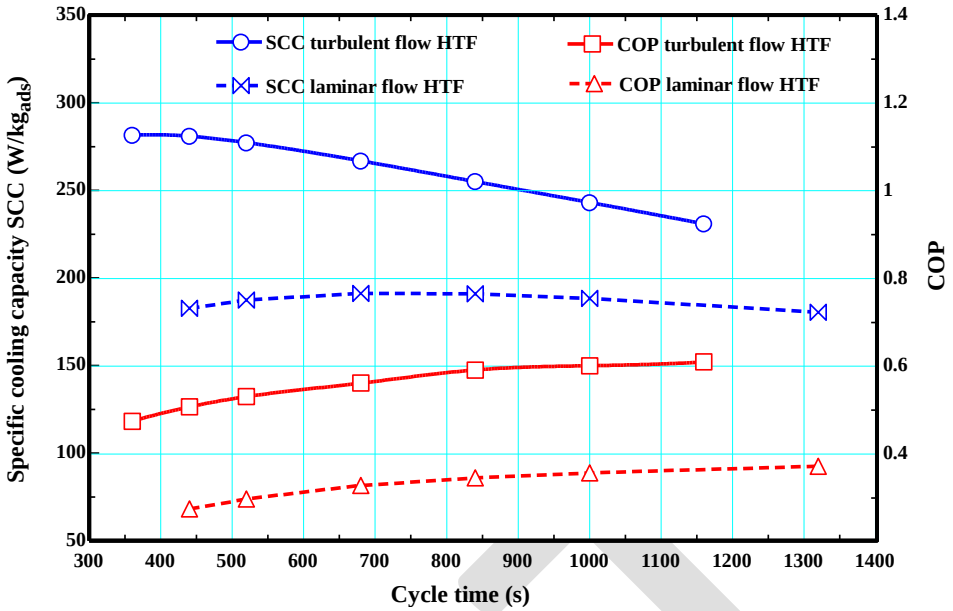

Fig. 4. Influence of cycle time on average specific cooling capacity and COP for the two cases: Laminar and turbulent HTF flow.

Table 2. Operating parameters of the HTF flow used in the simulations		
	Laminar flow	Turbulent flow
$u_{ave,hot,in}$	0.14 m/s	0.56 m/s
$u_{ave,cool,in}$	0.198 m/s	0.792 m/s
$\dot{m}_{hw}$	0.41418 kg/s	1.6567 kg/s
$\dot{m}_{cw}$	0.58577 kg/s	2.343 kg/s
$T_{hw,i}$	85 ^{o}C	85 ^{o}C
$T_{cw,i}$	31 ^{o}C	31 ^{o}C

It is clearly obvious that in case of turbulent flow of HTF both SCC and COP are considerably higher than their corresponding values for the laminar flow case for all selected cycle times. At a certain cycle time of 840 s the SCC and COP are increased by about 42% and 85% respectively when flow changed from the laminar to the turbulent regimes. In case of turbulent HTF, seven cycle times are examined as illustrated in Fig. 4 at (360, 440, 520, 680, 840, 1000 and 1160 s). The maximum cooling capacity or SCC at the shortest cycle times (360 s or 440 s) while the COP is the smallest. The COP increases monotonically with longer cycle times because of the time frame of the sensible heat consumed in the bed, particularly during the switching time, is reduced.

Fig. 5 shows the effect of this sensible heat at the start of pre-heating mode on the instantaneous heat added during a half cycle time for the cycle duration of 840 s.

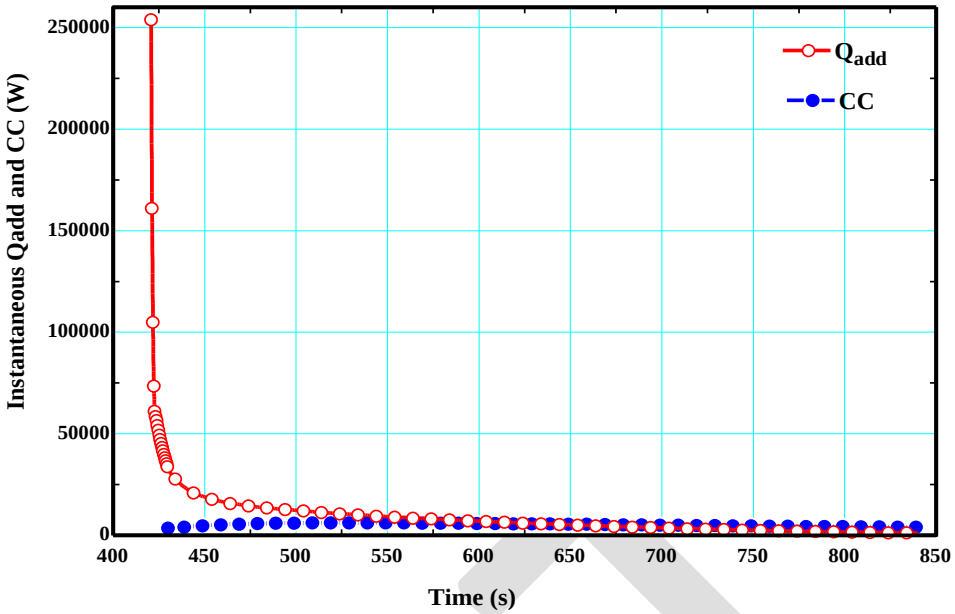

Fig. 5. Instantaneous cooling capacity during switching and adsorption modes for Bed-A, and heat added during switching and regeneration modes for Bed-B, for a half cycle time.

Although the pre-heating mode requires a short time (10 s in the given case), an extra-large energy is consumed, and that due to the sensible heat consumed in the bed which has just finished its cooling process before the switching mode. The pre-heating mode consumes about 18 % of the average heat added during the cycle for the given case; highlighting on the role of thermal masses of an adsorbent-bed. Fig. 6 presents the consumed heat after pre-heating mode and also shows clearly the variation in the instantaneous cooling capacity.

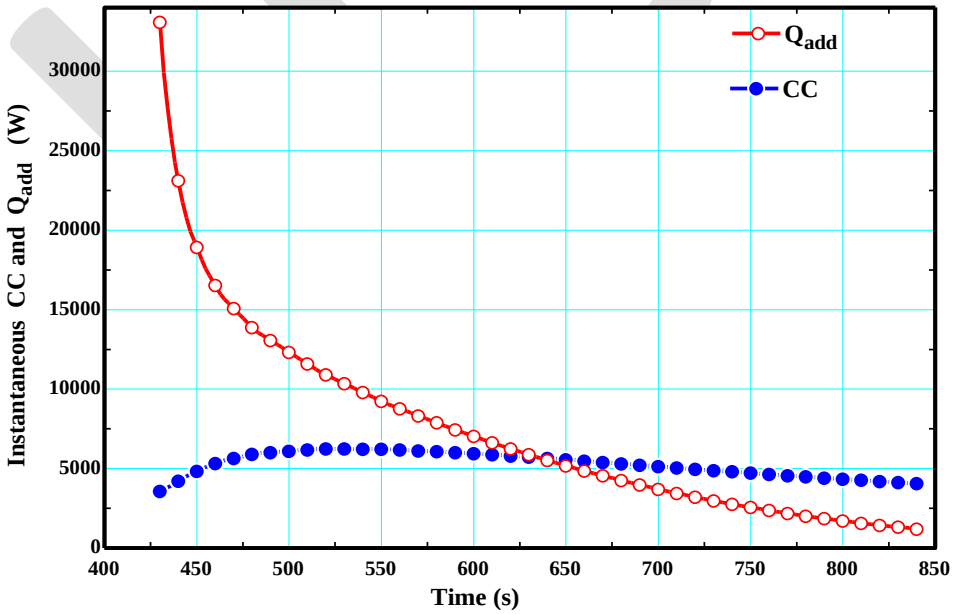

Fig. 6. Instantaneous cooling capacity during adsorption mode for Bed-A, and heat added during desorption mode for Bed-B.

The cycle duration of 840 s is chosen for the simulations and comparisons in the next figures, as it has an average COP about 0.5916 and SCC about 255 kg/kg$_{ads}$ for the case of turbulent flow HTF.

The variations in the average temperature, pressure and uptake in the adsorbent domain during a complete cycle are illustrated in Fig.7 for the two flow regimes cases. The average temperature of the adsorbent domain is in a wider range of change in case of turbulent HTF flow than that in case of laminar flow; accordingly the range of equilibrium amount of adsorbate is extended and then the performance is enhanced. Because of the pressures of the condenser and evaporator are not ideal, the pressure fluctuations in desorption/adsorption modes are obvious and more increased in the case of turbulent HTF flow; affected by the increase in refrigerant flow rate out/in the adsorber.

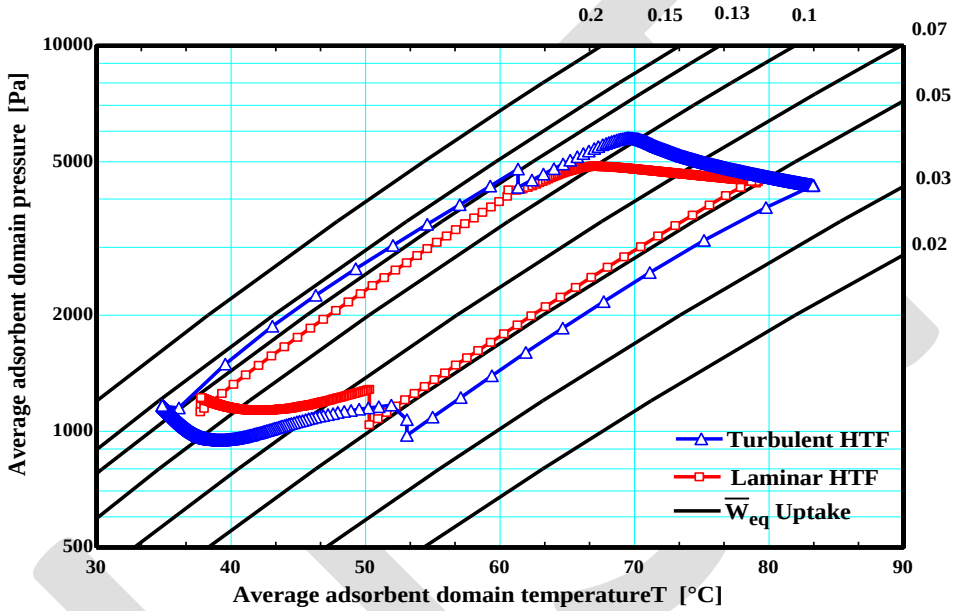

Fig. 7. The average P-T-W$_{eq}$ diagram of the adsorbent domain under cyclic steady state for the turbulent and laminar HTF flow regime cases.

The duration of modes in the two cases of the basic model for cycle time of 840 is given in Table 3.

Table 3. Modes durations

	Laminar flow	Turbulent flow
Adsorption /Desorption time	390 s	410 s
Switching time	30 s	10 s
Half cycle time	420 s	420 s

The differences between the average bed temperature and the inlet and outlet HTF temperatures for Bed-A are shown in Fig. (8 and 9) for both cases of laminar and turbulent HTF flow respectively. Due to the increasing in heat transfer of the HTF in case of turbulent flow, the temperature differences of HTF between inlet and leaving of the bed are considerably decreased

reaching to about 0.5 ^{o}C by the end of heating and cooling processes, and the average bed temperature becomes more close to the inlet HTF temperatures. However, there is a theoretical availability, particularly at the end of cooling process, to get better performances as long as the average bed temperature does not reach its heat transfer limits.

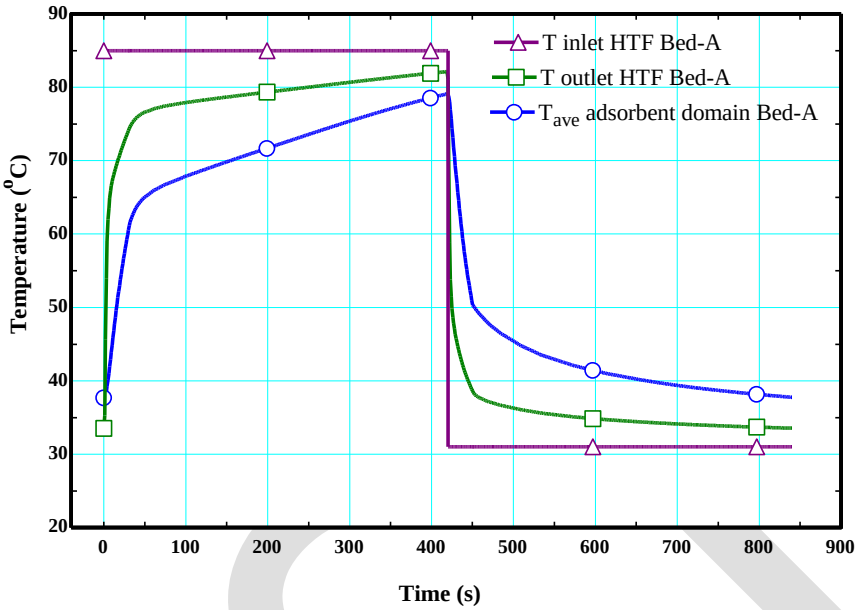

Fig. 8. The temperature histories for adsorbent domain , inlet and outlet HTF during steady state cycle (Bed-A) in case of laminar flow HTF

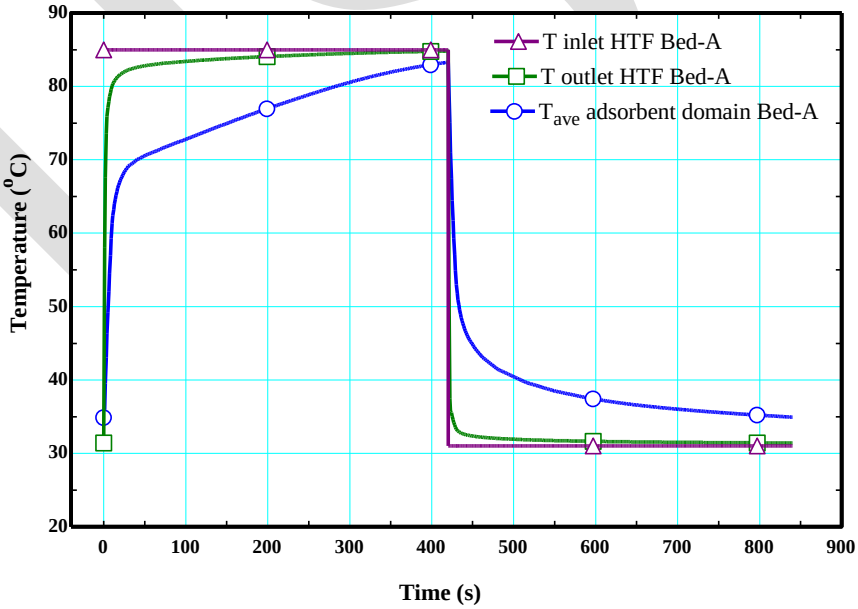

Fig. 9. The temperature histories for adsorbent domain , inlet and outlet HTF during steady state cycle (Bed-A) in case of Turbulent flow HTF

The relation between the average adsorbent domain pressure and the pressures of the condenser and evaporator are simulated in Fig. 10 and Fig. 11 for laminar and turbulent flows,

respectively. The pressure drop in vacuum chamber is very small, but it is more obvious during adsorption mode due to the increasing in vapor velocity at low pressures.

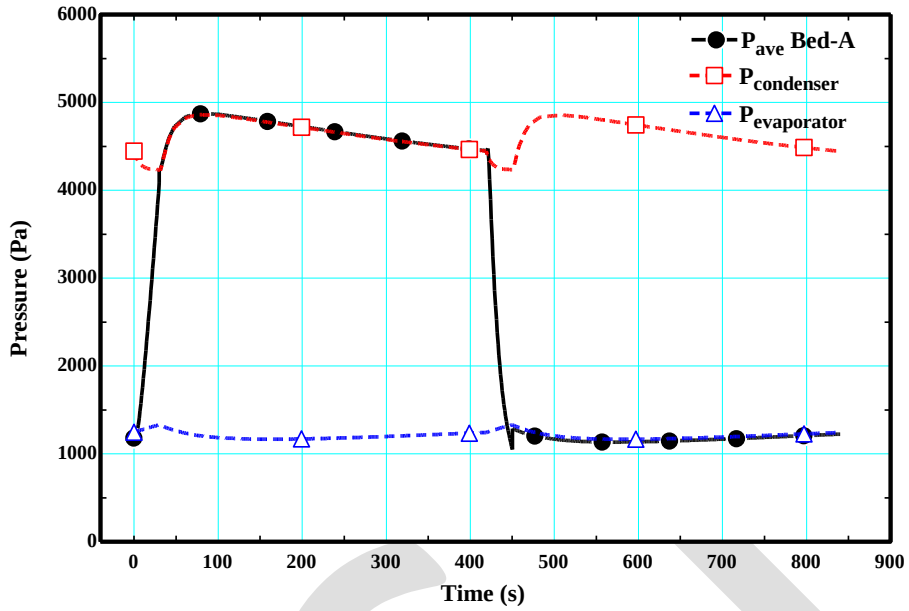

Fig. 10. The time variations of the average adsorbent bed pressure with the condenser and evaporator pressures in case laminar flow HTF for Bed-A

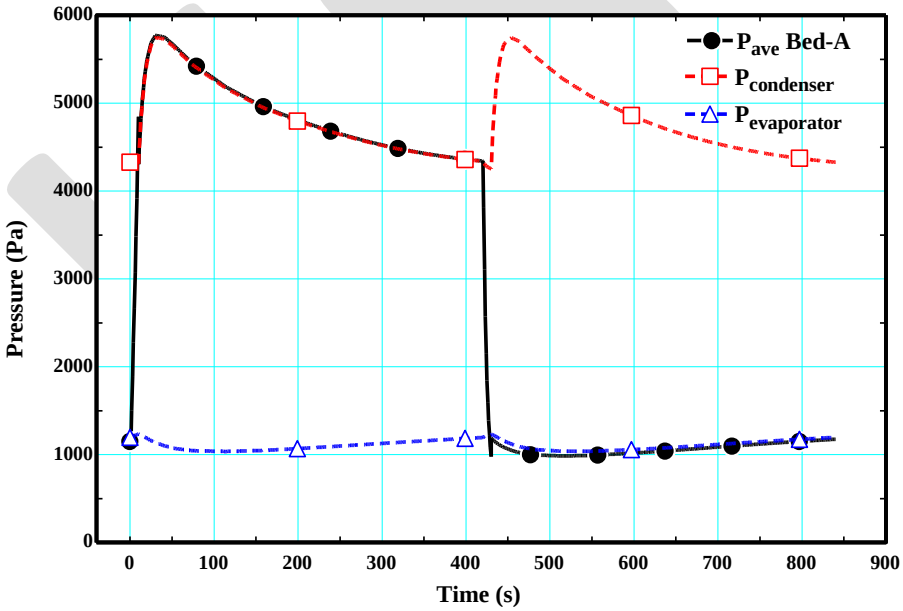

Fig. 11. The time variations of the average adsorbent bed pressure with the condenser and evaporator pressures in case Turbulent flow HTF for Bed-A

The local adsorption kinetic in the LDF equation depends on the difference between the equilibrium and instantaneous amount of adsorbate. Fig. (12 and 13) simulate those differences during a complete steady state cycle for the two beds for both cases of laminar and turbulent

flows, respectively. Basically, the diffusion of mass within the adsorbent particles is better with higher temperatures i.e. during desorption modes, that is why ($W_{eq} - w$) in desorption and adsorption modes are not identical during the steady state cycle. A larger difference is required during an adsorption mode to adsorb the same total amount desorbed during a desorption mode making cyclic steady state. Increasing the cooling water velocity or/and adsorption duration are the common ways to reach steady state cycle condition. It is important to mention that studying the net effect of any operating parameter on the adsorption kinetic during only one mode based on given initial conditions may lead to inaccurate predictions for the overall performance.

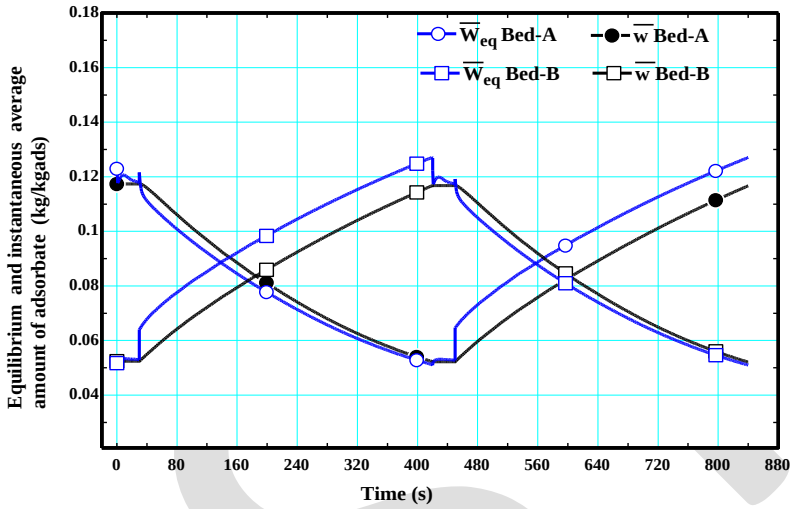

Fig. 12. The time variations of average equilibrium and instantaneous uptake in case of laminar HTF flow for the two beds.

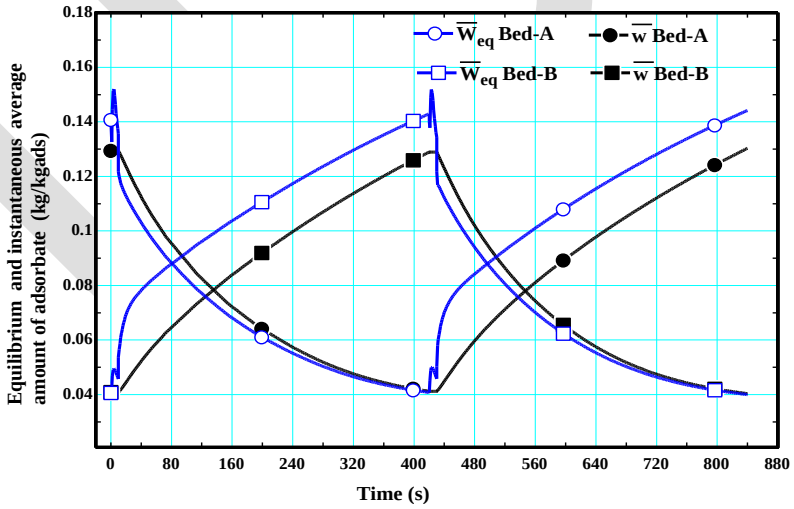

Fig. 13. The time variations of average equilibrium and instantaneous uptake in case of Turbulent HTF flow for the two beds.

In order to investigate the mass balance of the refrigerant within the cycle for the basic model in case of turbulent HTF flow, the time variations of the refrigerant mass flow rate and the adsorption kinetic are represented in Fig. (14 and 15), respectively. The figures prove that the rate of change in the average amount of adsorbate is consistent with

the refrigerant flow rate calculated at the valve openings by surface integration.

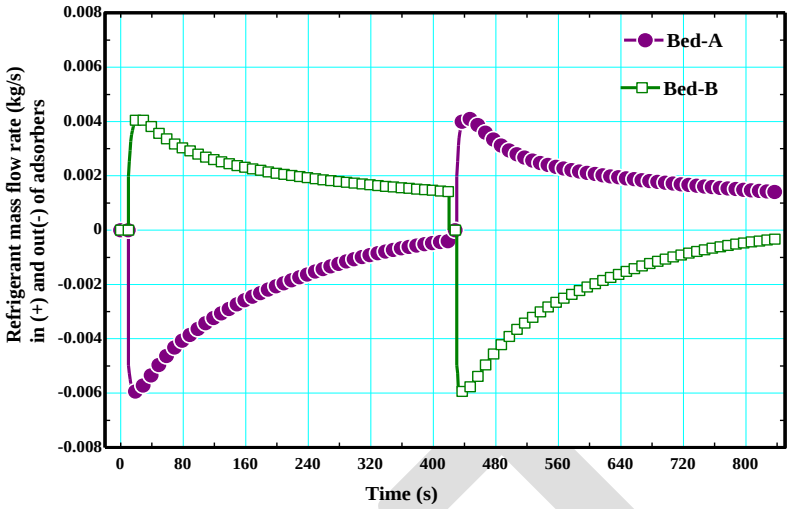

Fig 14. Shows the refrigerant mass flow rate for the two beds during steady state cycle.

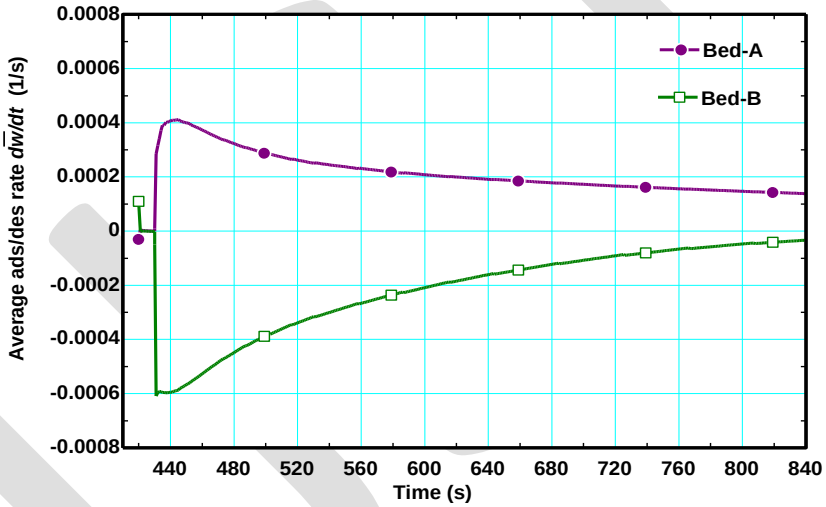

Fig. 15. Simulate the average adsorption kinetic during a half cycle for the two beds.

When the amount of adsorbent is considered in Fig.16, the comparability of the two ways used in calculating the refrigerant flow rate in and out of the adsorbers are clearly obvious and they are almost identical, and the differences due to the accumulation of vapor in the vacuum chamber can be hardly seen.

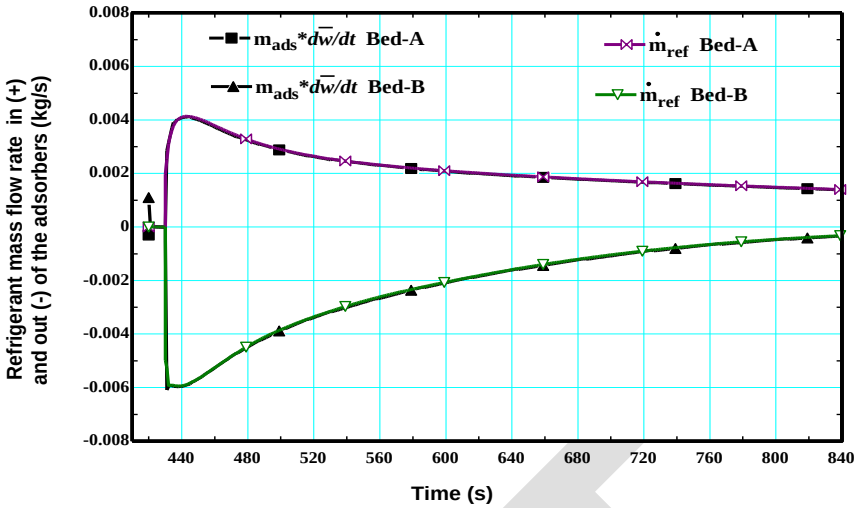

Fig. 16. Comparison between the two ways used in calculating the refrigerant mass flow rate.

Fig. 17 shows the effect of the HTF flow types on the average temperatures histories of the two beds' adsorbent-domains for the same inlet heating and cooling HTF temperatures and initial conditions. In both cases, the beds can be considered in the cyclic steady state after finishing the first three half cycles with minor changes in average temperatures about (0.1 ^{o}C). While the bed reaches it maximum average temperatures during desorption process of 83.2 ^{o}C and ^{o}C 79 ^{o}C for the cases of turbulent and laminar flows of HTF, respectively. In desorption mode while the beds under cooling, the minimum temperature reaches to (34.9 ^{o}C) in case of turbulent flow and (37.8 ^{o}C) in case of laminar HTF flow.

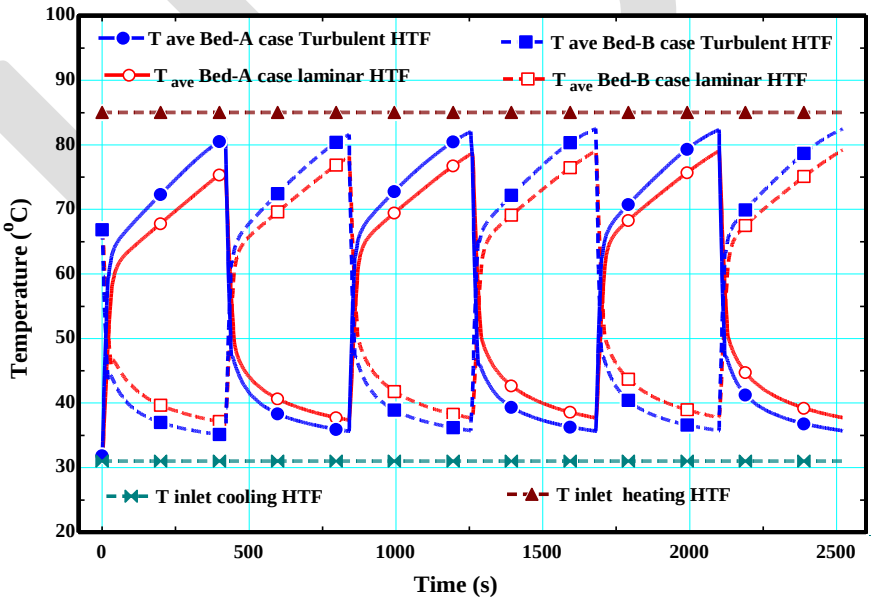

Fig. 17. The time variations of the average adsorbent domain temperatures for the two beds reaching to the cyclic steady state.

Fig. 18 shows the time variations of the leaving chilled water and cooling water

temperatures for the evaporator and condenser respectively. The entering chilled water and cooling water temperatures are set at fixed values. As the circulated refrigerant is increased with turbulent HTF flow, the evaporator performance is enhanced resulting in lower outlet chilled water temperatures than their corresponding temperatures for laminar HTF flow. In case of turbulent HTF flow, The minimum leaving chilled water temperature during cyclical steady state operation is 8.3 ^{o}C, while the average leaving chilled water temperature is 9.7 ^{o}C.

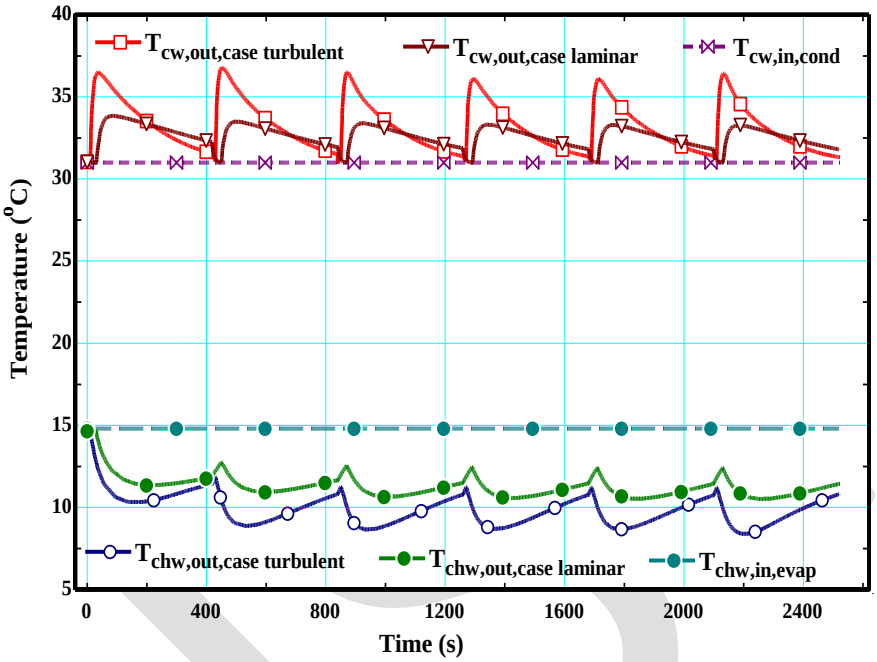

Fig. 18. The time variations of the chilled water and cooling water temperatures.

Conclusions

A fully coupled system of equations was successfully modeled for a two-bed adsorption chiller considering internal and external mass transfer resistances of the adsorbent particles in a backed-bed adsorber, and coupling the flow in adsorbent domain with that in vacuum chamber while the pressures of condenser and evaporator were not ideal. Furthermore, the modified volume-averaged Navier-Stokes equations were applied on the flow in the adsorbent domain, and both of the turbulent and laminar flow types for HTF were included in the model equations. Under the given operating and physical parameters, the following conclusions were drawn from the comparisons and simulations of the results:

- The HTF flow is strongly recommended to be turbulent flow rather than laminar flow because both of SCC and COP are greatly increased at all cycle times, and specifically at shorter cycle times. For example, at a cycle time of 840 s, SCC and COP are increased by about 42% and 85% respectively, when the flow of the HTF is changed from laminar to turbulent types.

- The adsorption durations can be extended to adsorb more refrigerant as the bed does not reach to its mass and heat transfer limits.
- The pressure drop in the vacuum chamber is generally very small. However, it is more obvious in adsorption modes than in desorption mode due the increasing in velocity of refrigerant at low pressures occurring in the adsorption process.
- The mass balance for the adsorbent bed is confirmed by using two different methods in calculating the refrigerant that entering and leaving the adsorbers; the first calculation from averaging the local kinetic rate within the adsorbent, and the second one from the surface integration at the valve opening.

References

[1] X. Wang, W. Zimmermann, K. C. Ng, A. Chakraboty, J. U. Keller, Investigation on the isotherm of silica gel-water systems: TG and volumetric methods, Journal of Thermal Analysis and Calorimetry, 76 (2004) 659–669.

[2] J. Deng, R.Z. Wang, G.Y. Han, A review of thermally cooling technologies for combined cooling heating and power systems. Progress in Energy and Combustion Science, 37(2) (2011), 172–203

[3] L. M. Sun, N. Ben Amar, F. Meunier, Numerical study on coupled heat and mass transfers in an adsorber with external fluid heating, Heat Recot, ery Systems & CHP , 15(I) (1995)19-29.

[4] H. T. Chua, K. C. Ng, W. Wang, C. Yap, X. L. Wang, Transient modeling of a two-bed silica gel-water adsorption chiller, International Journal of Heat and Mass Transfer, 47(4) (2004), 659-669.

[5] A. Sharafian, M. Claire, M. Bahrami, Impact of fin spacing on temperature distribution in adsorption cooling system for vehicle A/C applications, International Journal of Refrigeration,51 (2015), 135-143.

[6] L. Z. Zhang, L. Wang, Effects of coupled heat and mass transfers in adsorbent on the performance of a waste heat adsorption cooling unit, Applied Thermal Engineering, 19 (1999) 195-215.

[7] K.C. Leong, Y. Liu, Numerical modeling of combined heat and mass transfer in the adsorbent bed of a zeolite/water cooling system, Applied Thermal Engineering 24 (2004) 2359–2374.

[8] H. Niazmand, I. Dabzadeh, Numerical simulation of heat and mass transfer in adsorbent beds with annular fins, International Journal of Refrigeration, 35 (2012), 581-593.

[9] H. Niazmand, H. Talebian, M. Mahdavikhah, Bed geometrical specifications effects on the performance of silica/water adsorption chillers, International Journal of Refrigeration, 35 (2012), 2261-2274.

[10] M. Mahdavikhah, H. Niazmand, Effects of plate finned heat exchanger parameters on the adsorption chiller performance, Applied Thermal Engineering, 50 (2013) 939-949.

[11] Y. Liu, K.C. Leong, Numerical modeling of a zeolite/water adsorption cooling system with non-constant condensing pressure, International Communications in Heat and Mass Transfer, 35 (2008) 618–622.

[12] R. Z. Wang, Y. X. Xu, J. Y. Wu,W. Wang, Experiments on heat-regenerative adsorption refrigerator and heat pump, Int. J. Energy Res., 22 (1998) 935-941.

[13] A. Freni, A. Sapienza, I.S. Glaznev, Y. I. Aristov and G. Restuccia, Experimental testing of a lab-scale adsorption chiller using a novel selective water sorbent "silica modified by calcium nitrate", International Journal of Refrigeration, 35 (2012), 518-524.

[14] A. R. M. Rezk, Theoretical and experimental investigation of silica gel / water adsorption refrigeration systems, PhD. Thesis, University of Birmingham, 2012.

[15] B.B. Saha, I.I. El-Sharkawy, A. Chakraborty, S. Koyama, Study on an activated carbon fiber-ethanol adsorption chiller: Part II - performance evaluation, International Journal of Refrigeration, 30 (2007) 96-102.

[16] N. Ben Amar, L. M. Sun, F. Meunier, Numerical analysis of adsorptive temperature wave regenerative heat pump, Applied Thermal Engineering, 16(5) (1996), 405-418.

[17] M. Takahiko, I. El-Sharkawy, B.B. Saha, S. Koyama, Optimized performance of one-bed adsorption cooling system, 15th International Refrigeration and Air Conditioning Conference at Purdue, July (2014).

[18] A. Sakoda, M. Suzuki, Fundamental study on solar powered adsorption cooling system, Journal of Chemical Engineering of Japan, 17(1) (1984), 52-57.

[19] H. T. Chua, K. C. Ng, A. Malek, T. Kashiwagi, A. Akisawa, B. B Saha, Modeling the performance of two-bed, silica gel-water adsorption chillers, International Journal of Refrigeration, 22(3) (1999), 194-204.

[20] B. B. Saha, A. Chakraborty, S. Koyama, Y. I. Aristov, A new generation cooling device employing CaCl2-in-silica gel–water system, International Journal of Heat and Mass Transfer 52 (2009) 516–524.